FEAT

Canadian Nuclear Society
Société Nucléaire Canadienne

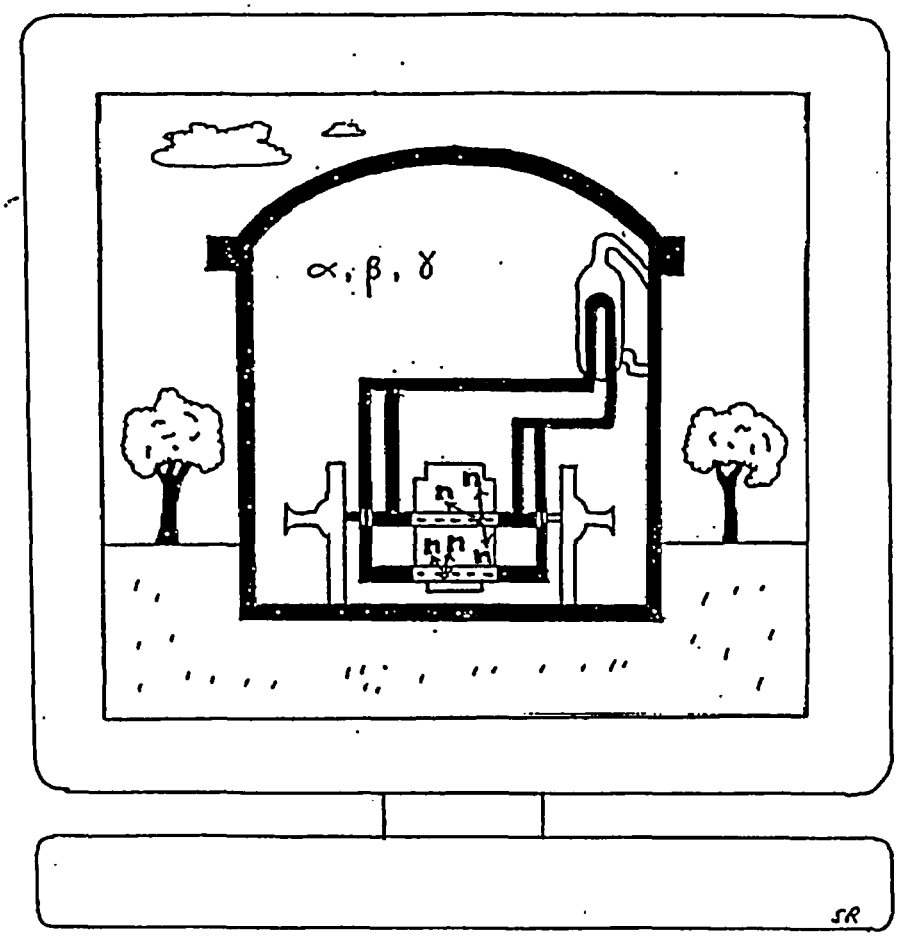

Proceedings, 19th Annual Conference
Comptes rendus, 19e congrès annuel
Toronto, Ontario, Canada
1998/10/18-21

Volume 2 of 2
2ième de 2 volumes

CNS Technical Program

Wednesday Oct. 21 09:00 - 12:00 Regency D Room

Session 4D Fuel

Chair: B.J. Lewis (Royal Military College)

09:00-09:25 A Standard Approach to Special Fuel Irradiations at Point Lepreau Generating Station, P.J. Reid (ALARA Research, Inc.), R.G. Steed, R.A. Gibb and R.W. Sancton (New Brunswick Power)

09:25-09:50 Validations, Verifications and Applications of the FEAT Code, Z. Xu, C. Manu, M. Tayal, and J.H. Lau (AECL)

09:50-10:15 Assessment of Fuel Fitness for Service Following Standing Start Process During Gentilly-2 Annual Outage, Q.M. Lei and P. Gulshani (AECL) and H. Huynh (Hydro-Québec)

10:15-10:45 Break

10:45-11:10 Investigation of Fuel-Bundle Vibration in the Chalk River Single-Channel Test Rig, V.P. Janzen, T.G. Whan, J.L. Gérardi, I.E. Oldaker, B.A.W. Smith, C.E. Taylor and J.H. Tromp (AECL)

Validations, Verifications and Applications of the FEAT Code

Z. Xu, C. Manu, M. Tayal, J.H. Lau

Atomic Energy of Canada Limited
2251 Speakman Drive, Mississauga, Ontario L5K 1B2

Abstract

The FEAT code (finite-element analysis for temperature), a general-purpose two-dimensional finite-element computer code for heat-flow calculations in solids of arbitrary shapes, is frequently used in thermal design and assessment of CANDU fuel. Examples of applications include high-burnup pellets (two-dimensional heat conduction in short pellets with big chamfers), effect of end flux peaking on peak pellet temperature, graphite disc fuel (two-dimensional heat transfer that is due to the existence of a highly conductive graphite disc between neighbouring pellets), pellet bottoming during load-following, sheath-bearing pad heat-transfer analysis for designing a bearing pad that eliminates crevice corrosion, and effect of pellet grooves for instrumentation and gas storage.

The FEAT code models both steady-state and transient two-dimensional heat conduction with internal heat generation; with user-specified boundary conditions (e.g., prescribed boundary heat convection, prescribed boundary heat fluxes and prescribed boundary temperatures); with variable material properties such as temperature dependence of thermal conductivity, specific heat and density (nonlinear heat conduction); and with gaps between different materials (heat conduction in multiple bodies).

A detailed validation and verification of the FEAT code was recently done using the validation-matrix approach, which included the following activities:

1. creating validation matrices that include scenario-to-phenomenon table that specifies phenomena expected to occur during scenarios, and phenomenon-to-data set table that associates the phenomena to data sets that can be used to validate the modelling of phenomena; identifying all the features in the FEAT code that need to be tested; searching for cases to test features; forming a test matrix that consists of 40 test cases based on the phenomena modelled, for example, the convergence test cases, steady-state cases, transient cases, etc. All the features of the FEAT code were covered by the test matrix.
2. finding independent solutions for all the test cases from analytical solutions, other codes and experimental measurements.
3. comparing the FEAT predictions with the independent solutions for each of the test cases.

This paper describes the results from this study. As well, some illustrative examples are given.

The differences between FEAT predictions and results from analytical solutions or other independent codes are generally within 3.0 %. This result shows that the FEAT code correctly handles the fundamentals of heat transfer that the code simulates. Isotherms calculated by FEAT are consistent with a number of experimental observations including tear-drop-shaped voids that are due to end flux peaking, grain growth profiles in graphite disc fuel and in grooved pellets, and measured temperatures in the sheath with bearing pad. Also, the study confirms that the FEAT code converges rapidly to the true solution, both in space and in time.

Introduction

FEAT is a general-purpose finite-element computer code that is used for calculating temperatures in solids of arbitrary shapes[1]. The code models both steady-state and transient[2] two-dimensional heat conduction, with internal heat generation, with user-specified boundary conditions (prescribed boundary heat convection, prescribed boundary heat fluxes, and prescribed boundary temperatures), with variable material properties such as temperature dependent thermal conductivity, specific heat and density (nonlinear heat conduction), and with gaps between different materials (heat conduction in multiple bodies). The FEAT code has been used in nuclear fuel design and analysis. Examples of applications include sheath bearing-pad heat-transfer analysis for designing a bearing pad that eliminates crevice corrosion; peak pellet temperature analysis during end flux peaking; and calculations of temperatures in nongrooved pellets, in grooved pellets, and in graphite disc fuels.

This paper describes the recently completed validation and verification activities for the FEAT code (version 3.0). This paper also presents the results of some typical cases from the validation activities as well as some illustrations of applications of the code for nuclear fuel-element heat-transfer analysis.

The FEAT Advantage

As mentioned above, FEAT is a general-purpose finite-element computer code for heat flow in single and multiple bodies. The FEAT code was developed for analysis of nuclear fuel for steady-state and transient conditions, and therefore includes features which optimize its performance for these applications compared to commercially available general-purpose finite-element computer codes:

- use of a simple triangular finite element;
- availability of algorithms for automatic generation of finite element meshes for CANDU fuel geometries demonstrated in Reference 2 and in the present paper to yield accurate results. These algorithms arrange the finite elements in hexagonal patterns shown to produce convergent results faster than any other arrangement[3];
- use of specific data bases for end flux peaking effects and for temperature-dependence of UO_2 thermal conductivity (e.g. MATPRO-9[4], MATPRO-11[5]) as well as for fuel with various burnups;
- continuous improvements of its technical capabilities (e.g. Reference 2);
- availability of well-designed postprocessing technical capabilities (capability to select output models within the code) that produce results specifically required for assessments of nuclear fuel behavior, like volume-averaged temperature values.

With these features, the FEAT computer code has the capability to accurately, effectively and economically meet the needs of developers, manufacturers and users of nuclear fuel. Below we present a few cases and applications from the validation and verification of the technical capabilities of the FEAT finite-element computer code.

Validation and Verification Matrices

Validation matrices, including 2 set of tables, were created: scenario-to-phenomenon table that specifies phenomena expected to occur during scenarios (Table 1), and phenomenon-to-data set

table that associates the phenomena to data sets that can be used to validate the modelling of phenomena (Table 2).

After all the features in the FEAT code were identified, cases were found to test these features, and a test matrix consisting of 40 cases was created. This matrix covers every feature in the FEAT code (see Table 2). For example, FEAT can solve a steady-state or transient heat-conduction problem with internal heat generation, in multiple bodies, with variable material properties, and so on. These features were tested separately in separate cases. Problems in different coordinate systems (x-y, r-z and r-θ coordinate systems) were also tested.

There are 4 series of test cases. Series 1 contains all the cases for steady-state heat conduction problems that can be solved analytically or by hand calculations; series 2 includes all the cases for transient heat-conduction problems that can be solved either analytically or by other independent computer codes (ANSYS, ELOCA); series 3 consists of test cases that can be compared with experimental measurements or observations; series 4 has the convergence test (for both mesh convergence and time convergence) cases that can be solved analytically.

Applications of the FEAT code are illustrated with discussion of the cases in series 3 that are comparisons with direct measurements of fuel pellet or fuel sheath temperature. Although the overall results will be summarized in the current paper, only a few typical cases are discussed in detail because of space considerations. In the section that follows, for each typical case a description will be given first, independent solutions will then be discussed, and finally the prediction from the FEAT code will be compared with the independent solution.

Comparisons between Independent Solutions and FEAT Predictions

Case 4-1: mesh convergence test for axisymmetric geometry
There is steady-state heat conduction in a long solid cylinder (radius R, thermal conductivity k), with internal heat generation q" and specified surface temperature T_s. Find the centreline temperature T_c.

(a) An analytical solution for this problem can be found in the open literature[6]. The centreline temperature is

$$T_C = T_S + \frac{q'' R^2}{4k}$$

Input parameters: $T_S = 1700$ °C, $q'' = 76.7 \times 10^6$ W/m^3, $k = 2.3$ W/m·°C, $R = 6 \times 10^{-3}$ m. The result of the analytical solution is $T_C = 2000.13$ °C.

(b) FEAT predictions: Hexagonal meshes, internally generated by the FEAT code, were used in FEAT predictions. FEAT predictions based on different meshes (different number of radial nodes) are compared with analytical solutions in Figure 1. It is seen that the FEAT code converges rapidly in space for axisymmetric problems.

Case 4-3: time convergence test for axisymmetric geometry:
There is transient radial heat conduction in a long solid cylinder (radius R, thermal conductivity k, density r, specific heat C_p). Initial temperature T_i is uniform. At time = 0, the temperature of the surrounding fluid T_f is suddenly decreased. Assuming heat-transfer coefficient h, find the temperature at a point (r/R) at a time instant t.

(a) Analytical solutions for this problem are available in graphic forms[6,7]: for given r/R, N_{FO} and N_{BI}, the dimensionless temperatures can be found from a chart.
Input parameters: $R = 6 \times 10^{-3}$ m, r/R = 0.4, k = 2.4 W/m·°C, C_p = 500J/kg·°C, $\rho = 10.6 \times 10^3$ kg/m^3, h = 400 W/m^2·°C, T_i = 2000°C, T_f = 300°C.

$$N_{FO} = \frac{\alpha t}{R^2} = \frac{kt}{\rho C_p R^2} = 0.01257862t, \quad N_{BI} = \frac{hR}{k} = 1.0$$

The chart shows that when $r/R = 0.4$, $\frac{1}{N_{BI}} = 1.0$ and $N_{FO} = 1.2845$, $\frac{T - T_f}{T_i - T_f}$ is equal to 0.150.

This analysis leads to t = 102.118 s and T = 555°C.

(b) FEAT predictions using different time steps: A mesh of 26 radial nodes was used. FEAT predictions of the temperature after 102.118 s are obtained using different time steps and are compared with analytical solutions in Figure 2. It is seen that the FEAT code converges rapidly in time.

Case 1-3: heat transfer in a finite cylinder
A finite solid cylinder has radius of R and length of L. Thermal conductivity of the cylinder is k. The surface at r = R is heated to the temperature of T_s while the 2 ends of the cylinder are kept at zero temperature (T_e). Find the temperature profiles at 2 different z values.

(a) An analytical solution for this problem (Figure 3) is available[8]:

$$T(r,z) = \frac{2}{L}\sum_{n=1}^{\infty} \frac{I_0(n\pi r/L)}{I_0(n\pi R/L)} \sin(\frac{n\pi z}{L}) \cdot \int_0^L f(z') \sin(\frac{n\pi z'}{L}) dz'$$

with $f(z) = T_s$ = constant, the integration part can be reduced to

$$\int_0^L f(z') \sin(\frac{n\pi z'}{L}) dz' = T_s \int_0^L \sin(\frac{n\pi z'}{L}) dz' = \frac{T_s L}{n\pi} \int_0^{n\pi} \sin v dv = \frac{T_s L}{n\pi} (-\cos v)\Big|_0^{n\pi} = \frac{2T_s L}{n\pi} (n = 1,3,5,\cdots\cdots)$$

thus giving the analytical solution of $T(r, z)$ in the solid cylinder:

$$T(r,z) = \frac{4T_s}{\pi} \sum_{n=1,3,5,\cdots}^{\infty} \frac{I_0(n\pi r/L)}{I_0(n\pi R/L)} \sin(\frac{n\pi z}{L}) \cdot \frac{1}{n}$$

Input parameters: $R = 6 \times 10^{-3}$ m, $H = 7.5 \times 10^{-3}$ m, k = 3.7 W/m·°C, T_s = 2000°C, T_e = 0°C. The results of the analytical solution are plotted in Figure 4.

(b) FEAT predictions: A hexagonal mesh of 17 nodes in radial direction and 21 nodes in axial direction was used. Boundary conditions are shown in Figure 3. FEAT predictions are compared with analytical solutions in Figure 4. The difference between the 2 solutions is within the range of (-0.42 %, 0.07%), and it is considered to be in excellent agreement.

Case 1-6: heat transfer in 2 concentric cylinders
There is a thin gap (at R_1) between inner and outer long circular cylinders. Heat (q") is generated in the inner cylinder (radius R_1, thermal conductivity k_1, density ρ_1, specific heat C_{p1}). Conductance (h_1) exists across the gap between the inner cylinder and the outer cylinder (radius R_2, thermal conductivity k_2, density ρ_2, specific heat C_{p2}). The outer cylinder is cooled by

surrounding fluid (T_f, h_2). Find the temperature profiles with r in the inner cylinder and in the outer cylinder.

(a) An analytical solution for this problem (Figure 5 (a)) can be derived as follows:
Governing equations and boundary conditions are

inner cylinder $q''+\frac{k_1}{r}\frac{d}{dr}(r\frac{dT^{(1)}}{dr})=0,$ $\left.\frac{dT^{(1)}}{dr}\right|_{r=0}$ *is finite*

outer cylinder $\frac{k_2}{r}\frac{d}{dr}(r\frac{dT^{(2)}}{dr})=0$

$$-k_2\left.\frac{dT^{(2)}}{dr}\right|_{r=R_2}\cdot 2\pi R_2 L = h_2\cdot(T_2^{(2)}-T_f)\cdot 2\pi R_2 L$$

$$-k_2\left.\frac{dT^{(2)}}{dr}\right|_{r=R_1} = -k_1\left.\frac{dT^{(1)}}{dr}\right|_{r=R_1}$$

across gap $$-k_1\left.\frac{dT^{(1)}}{dr}\right|_{r=R_1}\cdot 2\pi R_1 L = q''\cdot\pi R_1^{\,2} L = h_1\cdot(T_1^{(1)}-T_1^{(2)})\cdot 2\pi R_1 L$$

steady state $$-k_2\left.\frac{dT^{(2)}}{dr}\right|_{r=R_2}\cdot 2\pi R_2 L = -k_1\left.\frac{dT^{(1)}}{dr}\right|_{r=R_1}\cdot 2\pi R_1 L = q''\cdot\pi R_1^{\,2} L$$

The solution is obtained by integrating the differential equations and finding integration constants:

$$T^{(2)} = C_1^{(2)}\ln r + C_2^{(2)}, \text{ where } C_1^{(2)} = -\frac{R_1^{\,2}q''}{2k_2} \text{ and}$$

$$C_2^{(2)} = T_f + \frac{R_1^{\,2}q''}{2R_2h_2} + \frac{R_1^{\,2}q''}{2k}\ln R_2$$

$$T^{(1)} = -\frac{q''}{4k_1}r^2 + C_2^{(1)}, \text{ where}$$

$$C_2^{(1)} = T_f + R_1^{\,2}q''(\frac{1}{2R_2h_2} + \frac{1}{2k_2}\ln\frac{R_2}{R_1} + \frac{1}{2R_1h_1} + \frac{1}{4k_1})$$

Input parameters: $R_1 = 6\times10^{-3}$ m, $R_2 = 8\times10^{-3}$ m, $k_1 = 3.7$ W/m·°C, $k_2 = 12.18$ W/m·°C, $h_1 = 1.0\times10^4$ W/m²·°C, $h_2 = 2.0\times10^4$ W/m²·°C, $T_f = 0$°C, q'' $= 2.18\times10^8$ W/m³. The results of the analytical solution are plotted in Figure 6.

(b) FEAT predictions: A hexagonal mesh (8 and 3 nodes in radial direction in inner bar and in outer bar, 10 nodes in axial direction) was used. Boundary conditions are as shown in Figure 5 (b). Results of the FEAT prediction and comparison with the analytical solution are illustrated in Figure 6. The difference between the 2 solutions is within the range of (-0.09%, 0.6%), and again it is considered to be in excellent agreement.

Case 2-6: transient heat conduction in a semi-infinite slab
A semi-infinite slab has constant density ρ, specific heat C_p and thermal conductivity k. The slab is initially at zero temperature (T_i). At time = 0, heat is generated in the slab (q''). The surface at

$x = 0$ is maintained at zero temperature ($T_w = 0$). Find the temperature profiles in the slab for the different time instants.

(a) Analytical solution for this problem (Figure 7 (a)) can be found in the literature[8]. Governing equation and boundary conditions are

$$\frac{\partial^2 T}{\partial x^2} + \frac{q''}{k} = \frac{1}{\alpha}\frac{\partial T}{\partial t}$$

$$T|_{x=0} = 0$$

$$T_i|_{t=0, x>0} = a + bx$$

The analytical solution for temperature T is

$$T = (a + \frac{\alpha \cdot q'' t}{k} + \frac{q'' x^2}{2k}) erf(\frac{x}{2\sqrt{\alpha \cdot t}}) + \frac{q'' x}{k}\sqrt{\frac{\alpha \cdot t}{\pi}} e^{\frac{x^2}{4\alpha \cdot t}} + bx - \frac{q'' x^2}{2k}$$

where $erf(\frac{x}{2\sqrt{\alpha \cdot t}}) = \frac{2}{\sqrt{\pi}} \int_0^{\frac{x}{2\sqrt{\alpha \cdot t}}} e^{-\xi^2} d\xi$

In the present problem, $a = 0$, $b = 0$, $T_i = 0$, the solution for temperature is reduced to

$$T = (\frac{\alpha \cdot q'' t}{k} + \frac{q'' x^2}{2k}) erf(\frac{x}{2\sqrt{\alpha \cdot t}}) + \frac{q'' x}{k}\sqrt{\frac{\alpha \cdot t}{\pi}} e^{\frac{x^2}{4\alpha \cdot t}} - \frac{q'' x^2}{2k}$$

Input parameters: $\rho = 10.0 \times 10^3$ kg/m^3, $C_p = 500$ J/kg·°C, $k = 3.7$ W/m·°C, $T_i = T_w = 0$°C, $q'' = 2 \times 10^8$ W/m^3. The temperature profiles at different time instants from the analytical solution are plotted in Figure 8.

(b) FEAT predictions: A hexagonal mesh with 17 nodes in x direction (6.0 mm) and 21 nodes in y direction (7.5 mm) was used. Boundary conditions are as shown in Figure 7 (b). FEAT predictions are compared with analytical solution in Figure 8. Both solutions are in very good agreement (the differences from both calculations are in the range of (-2.44%, 0.47%)).

Case 2-9: heat conduction with time-dependent heat generation
An infinite circular cylinder (radius R) is initially at temperature T_i. At time = 0, heat is generated in the cylinder ($q''' = q'''(t)$). The surface (at $r = R$) is cooled by surrounding fluid (T_f), and the heat-transfer coefficient between the cylinder and fluid is h. Assume that the cylinder has constant properties (thermal conductivity k, density ρ and specific heat C_p). Find the temperature profiles in the cylinder for the different time instants.

(a) The ANSYS code was used to provide an independent solution for this problem. The boundary conditions are shown in Figure 9. A hexagonal mesh with 17 nodes in radial direction (6.0 mm) and 21 nodes in axial direction (7.5 mm) was used. Input parameters: $R = 6 \times 10^{-3}$ m, $T_i = 300$°C, $q''' = 10^6 \times 500(1 + 0.025t)$ W/m^3, $T_f = 300$°C , $h = 2 \times 10^4$ W/m^2·°C, $k = 3.7$ W/m·°C, $\rho = 10 \times 10^3$ kg/m^3, $C_p = 500$ J/kg·°C. ANSYS predictions are plotted in Figure 10.

(b) FEAT predictions: The same hexagonal mesh was used. The same boundary conditions were applied. FEAT predictions are compared with the ANSYS solution in Figure 10. The differences from both calculations are in the range of (0.0%, 0.18%)). It is considered to be excellent agreement.

Case 2-14: centreline temperatures, as predicted by FEAT and ELOCA
Find the centreline temperature variation of CANDU fuel (a sheathed pellet) with time during power pulse. No flux peaking and no axial heat conduction are considered. Typical values are used for heat-transfer coefficients for pellet and sheath, sheath and coolant and power pulse.

(a) The ELOCA code was used to provide an independent solution for this problem[2]. The mesh is shown in Figure 11. ELOCA predictions are plotted in Figure 12.

(b) FEAT predictions: The same mesh was used. The same boundary conditions were applied. FEAT predictions are compared with the ELOCA solution in Figure 12. The difference between the 2 solutions is within the range of (-0.75%, 2.2%).

The overall comparison of FEAT predictions with independent solutions (obtained from analytical solutions, other independent computer codes) is summarized in Figure 13, which shows that all the FEAT-predicted temperatures are almost on the diagonal line. The differences between FEAT predictions and results from analytical solutions or other independent codes are within 3.0%.

Application of the FEAT code

The FEAT code can be used for thermal design and assessment. Two examples will be discussed here to illustrate the application of the FEAT code: effect of end flux peaking on pellet temperature distribution, and heat-transfer analysis for the area near the fuel sheath and bearing pad interface.

Case 3-2: end-flux-peaking–induced tear-drop–shaped void
Compare the predicted isotherms with the end-flux-peaking–induced tear-drop-shaped voids in fuel pellets (observed from neutron radiograph of some fuel elements from bundle GB).

(a) Neutron radiographs have indicated tear-drop-shaped voids in some of the fuel elements[1] (Figure 14). These voids occurred near fuel element ends after prolonged operation at high power. End-flux-peaking–induced axial temperature variation is responsible for the formation of the voids. The voids are believed to be associated with the temperature above 2100°C[1].

(b) FEAT predictions: The mesh used is the same mesh that is shown in Figure 11. A typical end flux peaking profile for CANDU fuel (Figure 15) was used. Figure 14 shows predicted isotherms, and they have the same shape as experimentally observed voids.

Case 3-3: thermocouple measurement near the sheath–bearing-pad interface
Compare the predicted temperatures with those obtained from the thermocouple measurement near a bearing pad.

(a) An experimental measurement of temperatures in the pressure tube in contact with the bearing pad of a sheath is available[1] (Figure 16). In the experiment, a heat flux of 110 W/cm^2 was applied on the inner surface of the sheath. The thermocouple-measured temperatures were between 310°C and 311°C for the point near pressure tube inner surface (near bearing pad) and between 303°C and 304°C for the point near the pressure tube outer surface (away from bearing pad).

(b) FEAT predictions: The mesh used contains 310 finite elements and 199 nodes (Figure 16). Boundary conditions are also shown in Figure 16. The predicted temperatures for the 2 locations are 310.20°C and 303.85°C respectively. They are very close to the measurement. An isotherm plot (Figure 17) is also given to show the temperature distribution.

Conclusions

A detailed validation of the FEAT code was performed using the validation-matrix approach. Validation matrices containing scenario-to-phenomenon and phenomenon-to-data set tables were created. The data set used for validation consists of analytical solutions, solutions from other codes and experimental measurements. Some verifications were also conducted, for example, test for both mesh convergence and time convergence. Forty cases listed in the test matrix, which covers all the features in the FEAT code were used. The convergence tests confirmed that the FEAT code converges rapidly to the true solution, both in space and in time. For 20 cases out of the 27 cases in which direct comparisons in temperature calculations can be made, predictions from FEAT are in excellent agreement (1.0%) with independent solutions (see Figure 18). General FEAT predictions are within 3.0% of the results of the analytical solutions or of other independent codes. This validation shows that the FEAT code handles fundamentals of heat transfer correctly. The FEAT code is also able to predict tear-drop-shaped voids that are due to end flux peaking and temperature distribution in the sheath with bearing pad. The predicted isotherms are consistent with the experimental observations.

Acknowledgements

Authors gratefully acknowledge R. Aboud and Q. M. Lei for reviewing this manuscript and for providing analytical solutions for some of the test cases respectively.

Nomenclature

C_p	specific heat (J/kg·°C)
h	heat-transfer coefficient (W/m^2·°C)
H	height of a rectangular slab (m)
I_i, J_i	Bessel function of ith order
k	thermal conductivity (W/m·°C)
L	length of rectangular slab or cylinder (m)
N_{BI}	Biot modulus $N_{BI} = hR/k$ (for cylinder) or $N_{BI} = hL/k$ (for slab)
N_{FO}	Fourier modulus $N_{FO} = \alpha t/R^2$ (for cylinder) or $N_{FO} = \alpha t/L^2$ (for slab)
q	heat flux (W/m^2)
q‴	internal heat generation rate (W/m^3)
r	radial distance from cylinder centre (m)
R	radius of cylinder (m)
t	time (s)
T	temperature (°C)
x, y	coordinates (m)

Greek symbols

α	thermal diffusivity $\alpha = k/(\rho c)$ (m^2/s)
δ	penetration depth or thickness of an infinite slab (m)

Δ	differences between FEAT predictions and reference solutions (%)
γ, β	constant in thermal conductivity formulae
θ	angular coordinate
ρ	density (kg/m^3)

superscripts

(1), (2) *in region 1 or region 2*

subscripts

0, i	initial
s,w	at cylinder surface or slab wall
c	at centreline or centre plane
1,2	in region 1 or region 2
e	at cylinder end
f	fluid

References

1 M. Tayal, "The Finite Element Code FEAT to Calculate Temperatures in Solids of Arbitrary Shapes", Nuclear Engineering and Design, Vol. 114, 1989, pp. 99-114.

2 M. Tayal, S.D. Yu, C. Manu, R. Aboud, D. Bowslaugh and L. Flatt, "Modelling Transient Two-Dimensional Non-Linear Temperatures in Nuclear Fuel Using the FEAT Code", Proceedings of the 5th Internal Conference on CANDU Fuel, Toronto, Canada, 1997, pp.352-363.

3 T. Udoguchi, H. Okamura, T. Kan and Y. Nozeu, "An Error Analysis of Various Finite Element Patterns", Bulletin of JSME, 16, 1973, 102, pp. 1803-1813.

4 "MATPRO-Version 09: A Handbook of Materials Properties for Use in the Analysis of Light Water Reactor Fuel Rod Behavior", Edited and compiled by P.R. MacDonald and L.B. Thompson, Report TREE-NUREG-1005, EG&G Idaho, Inc., 1976.

5 "MATPRO-Version11(Revision 2): A Handbook of Materials Properties for Use in the Analysis of Light Water Reactor Fuel Rod Behavior", edited by D.L. Hagrman, G.A. Reyman and R.E. Mason, EG&G Idaho, Inc. NUREG/CR-0479, TREE-1280, Rev. 2, R3 and R4, 1981.

6 A.J. Chapman, "*Heat Transfer*", 3rd edition, Macmillan Publishing Co., Inc., New York, 1974.

7 L.M.K. Boelter, V.H. Cherry, H.A. Johnson and R.C. Martinelli, "*Heat Transfer Notes*", McGraw-Hill, New York, 1965.

8 H.S. Carslaw and J.C. Jaeger, "*Conduction of Heat in Solids*", 2nd edition, Oxford University Press, London, 1959.

Table 1 Validation Matrix: Scenario-to-Phenomenon

Scenario	Phenomenon	
scenario 1: peak pellet temperature during end flux peaking	1	heat conduction in cylindrical coordinate system
	2	multiple bodies with gaps
	3	variable thermal conductivity (temperature dependent)
	4	time-dependent internal heat generation
	5	convective boundaries
scenario 2: sheath-bearing pad heat transfer	1	heat conduction in Cartesian coordinate system
	2	multiple bodies with gaps
	3	two-dimensional temperature profiles
	4	variable thermal conductivity (temperature dependent)
	5	surface flux
	6	adiabatic boundaries
	7	convective boundaries
scenario 3: heat transfer in graphite disc fuel	1	heat conduction in cylindrical coordinate system
	2	multiple bodies with gaps
	3	two- dimensional temperature profiles
	4	variable thermal conductivity (temperature dependent)
	5	time-dependent internal heat generation
	6	adiabatic boundaries
	7	convective boundaries
scenario 4: pellet temperature with or without pellet bottoming	1	heat conduction in cylindrical coordinate system
	2	multiple bodies with gaps
	3	one- or two- dimensional temperature profiles
	4	variable thermal conductivity (temperature dependent)
	5	time-dependent internal heat generation
	6	convective boundaries

Table 2 Validation Matrix: Phenomenon-to-Data Set

	Phenomenon	Data Set
cylindrical coordinate system		
1.	heat conduction in cylindrical coordinate system	case 1-3, case 1-4, case 1-6, case 1-8, case 2-2, case 2-3, case 2-7, case 2-9, case 2-10, case 2-12, case 2-14, case 3-2, case 3-4.
2.	multiple bodies with gaps	case 1-6, case 2-12, case 2-14, case 3-2, case 3-4.
3.	two- dimensional temperature profiles	case 1-3, case 2-3, case 3-2, case 3-4.
4.	variable thermal conductivity (temperature dependent)	case 1-8, case 2-10, case 2-14, case 3-2, case 3-4.
5.	time- dependent internal heat generation	case 2-9, case 2-14.
6.	adiabatic boundaries	case 1-4, case 1-6, case 1-8, case 2-2, case 2-7, case 2-9, case 2-10, case 2-12, case 2-14, case 3-2, case 3-4
7.	convective boundaries	case 1-4, case 1-6, case 2-2, case 2-3, case 2-9, case 2-10, case 2-12, case 2-14, case 3-2, case 3-4.
Cartesian coordinate system		
1.	heat conduction in Cartesian coordinate system	case 1-1, case 1-2, case 1-5, case 1-7, case 1-10, case 2-1, case 2-4, case 2-5, case 2-6, case 2-8, case 2-11, case 3-1, case 3-3.
2.	multiple bodies with gaps	case 1-5, case 2-11, case 3-3.
3.	two- dimensional temperature profiles	case 1-2, case 1-10, case 2-4, case 3-1, case 3-3.
4.	variable thermal conductivity (temperature dependent)	case 1-7, case 1-10, case 2-5, case 3-1, case 3-3.
5.	surface flux	case 1-10, case 2-5, case 3-3.
6.	adiabatic boundaries	case 1-1, case 1-5, case 1-7, case 1-10, case 2-1, case 2-5, case 2-6, case 2-8, case 2-11, case 3-3.
7.	convective boundaries	case 1-1, case 1-5, case 1-10, case 2-1, case 2-11, case 3-1, case 3-3.

Table 3 Feature-based Test Matrix

Feature	Steady-State		Transient	
	axisymmetric	plane	axisymmetric	plane
	cylindrical coordinate system (r,z)	Cartesian coordinate system (x,y)	cylindrical coordinate system (r,z)	Cartesian coordinate system (x,y)
(1). convergence	case 4-1	case 4-2	case 4-3	case 4-4
(2). heat conduction	case 1-3, case 1-4 case 1-6, case 1-8 case 3-2, case 3-4	case 1-1, case 1-2 case 1-5, case 1-7 case 1-10, case 3-1 case 3-3	case 2-2, case 2-3 case 2-7, case 2-9 case 2-10,case 2-12 case 2-14	case 2-1, case 2-4 case 2-5, case 2-6 case 2-8, case 2-11
(3). internal heat source or sink	case 1-6, case 1-8 case 3-2, case 3-4	case 1-1, case 1-5 case 3-1	case 2-7, case 2-12	case 2-6, case 2-11
(4). time-dependent internal heat source or sink.	n/a	n/a	case 2-9, case 2-14	case 2-8
(5). gap/multiple bodies.	Case 1-6, case 3-2 case 3-4	case 1-5, case 3-1 case 3-3	case 2-12, case 2-14	case 2-11
(6). variable properties k^*, C_p^* etc.	case 1-8, case 3-2 case 3-4	case 1-7, case 1-10 case 3-1, case 3-3	case 2-10, case 2-14	case 2-5
(7). Two-dimensional profiles	case 1-3, case 3-2 case 3-4	case 1-2, case 1-10 case 3-1, case 3-3	case 2-3	case 2-4
(8). Adiabatic BC*	case 1-4, case 1-6 case 1-8, case 3-2 case 3-4	case 1-1, case 1-5 case 1-7, case 1-10 case 3-3	case 2-2, case 2-7 case 2-9, case 2-10 case 2-12,case 2-14	case 2-1, case 2-5 case 2-6, case 2-8 case 2-11
(9). Surface flux	case 1-4	case 1-10, case 3-3	case 2-3	case 2-5
(10). Surface temperature	case 1-3, case1-8	case 1-2, case 1-7 case 1-10	case 2-7	case 2-4, case 2-6, case 2-8
(11). Convective BC	case 1-4, case 1-6 case 3-2, case 3-4	case 1-1, case 1-5 case 1-10, case 3-1 case 3-3	case 2-2, case 2-3 case 2-9, case 2-10 case 2-12,case 2-14	case 2-1, case 2-11
(12). Central hole	case 1-4	n/a	case 2-3	n/a
(13). Polar coordinate system (r,θ)	case 1-9	n/a	case 2-13	n/a
(14). heat generation in pellets	case 1-13, case 3-2 case 3-4	n/a	case 2-14	n/a
(15). Thermal conductivity of UO_2	case 1-11			
(16). Thermal conductivity of Zircaloy	case 1-12			
(17). link with ELDAT file	case 1-14	n/a	case 2-14	n/a
(18). link with CONTOUR code	case 1-15	case 1-16	case 2-15	case 2-16

* k is thermal conductivity of material.
C_p is specific heat of material.
BC is boundary condition(s).
series 1: steady-state capabilities.
series 2: transient capabilities.
series 3: comparison with measurements.
series 4: convergence test.
n/a: not applicable.

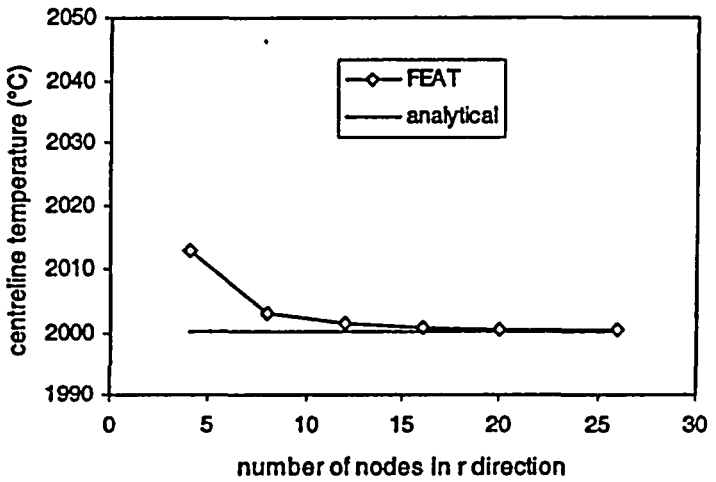

Figure 1 Mesh Convergence of FEAT (Case 4-1)

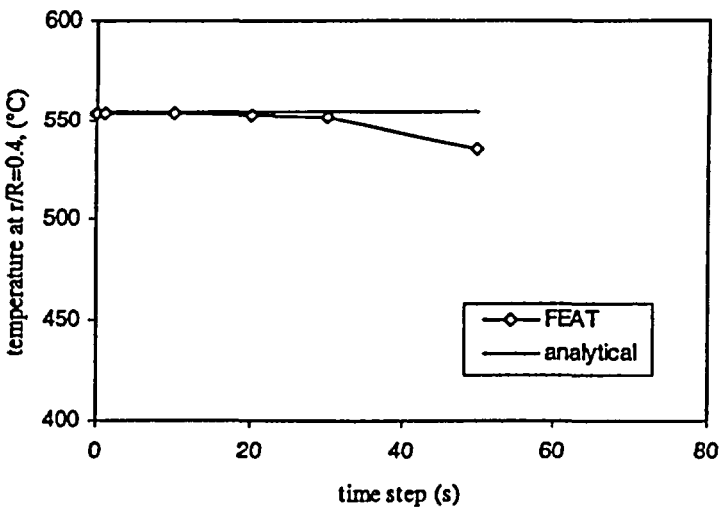

Figure 2 Time Convergence of FEAT (Case 4-3)

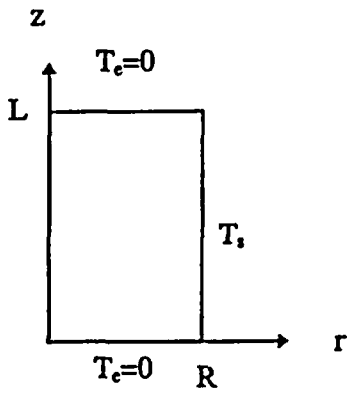

Figure 3 Heat Transfer in a Finite Cylinder (Case 1-3)

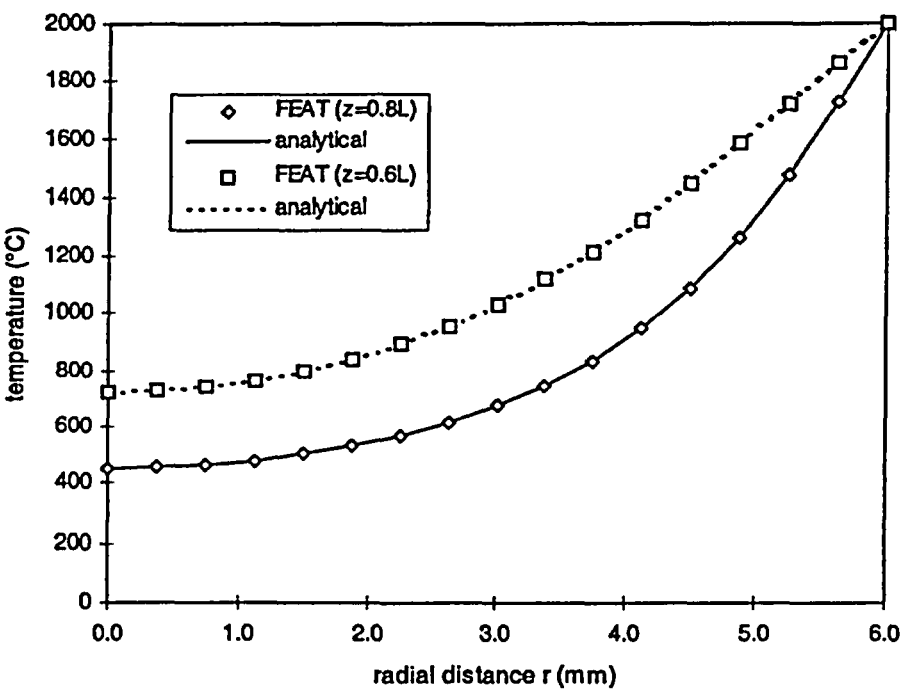

Figure 4 Two-dimensional Temperature Distribution (Case 1-3)

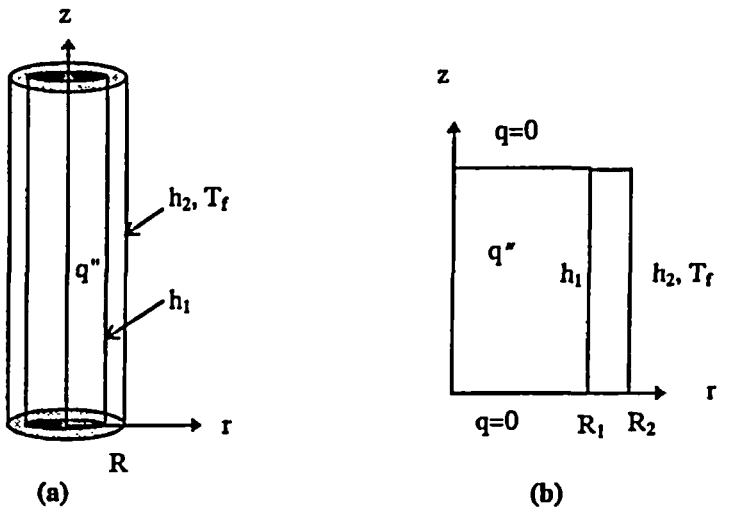

Figure 5 Heat Transfer in Two Concentric Cylinders (Case 1-6)

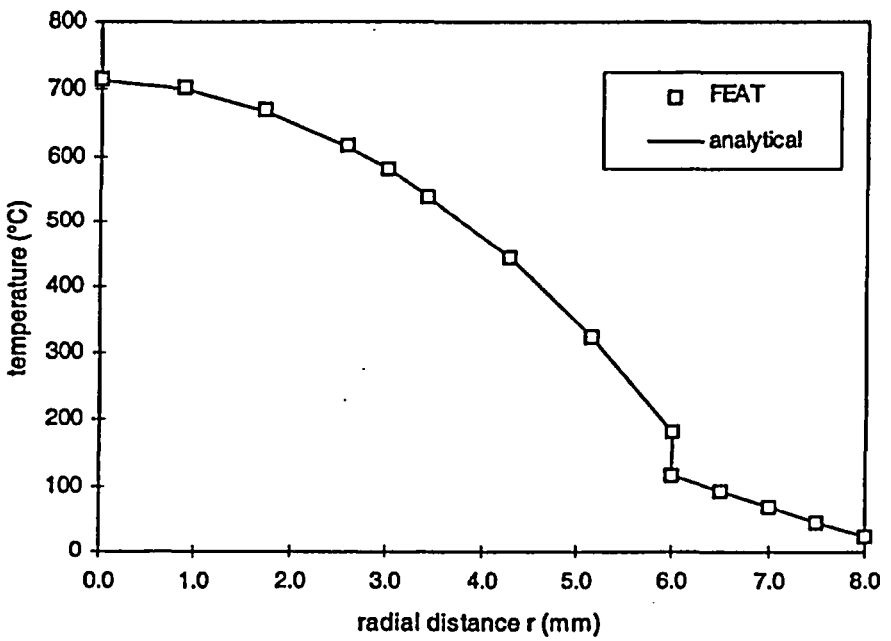

Figure 6 Temperature Profiles (Case 1-6)

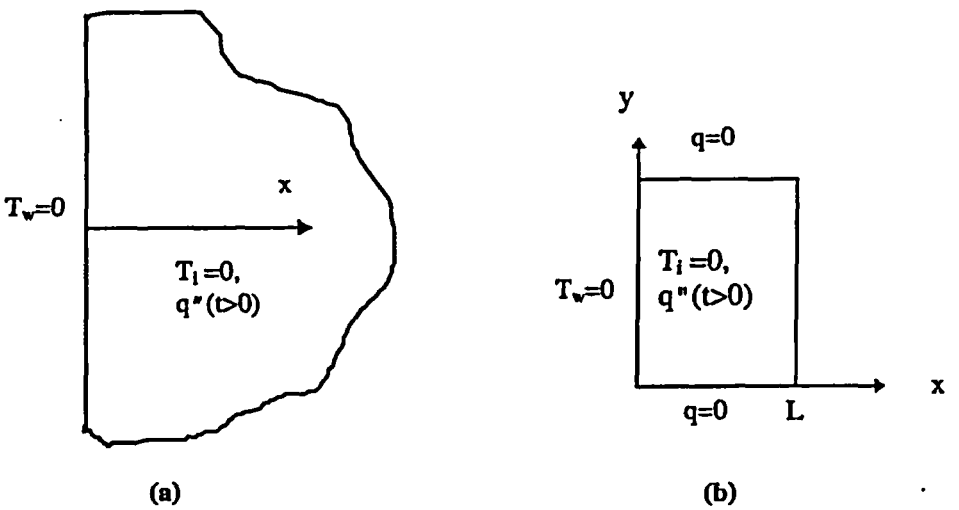

Figure 7 Transient Heat Conduction in a Semi-infinite Slab (Case 2-6)

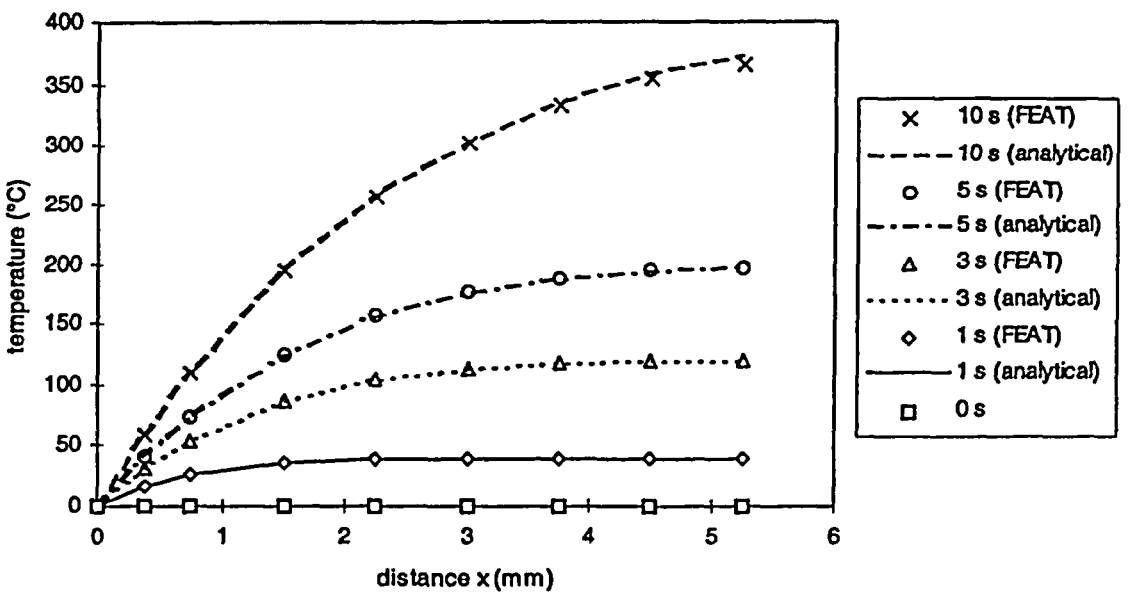

Figure 8 Temperature Profiles for Different Time Instants (Case 2-6)

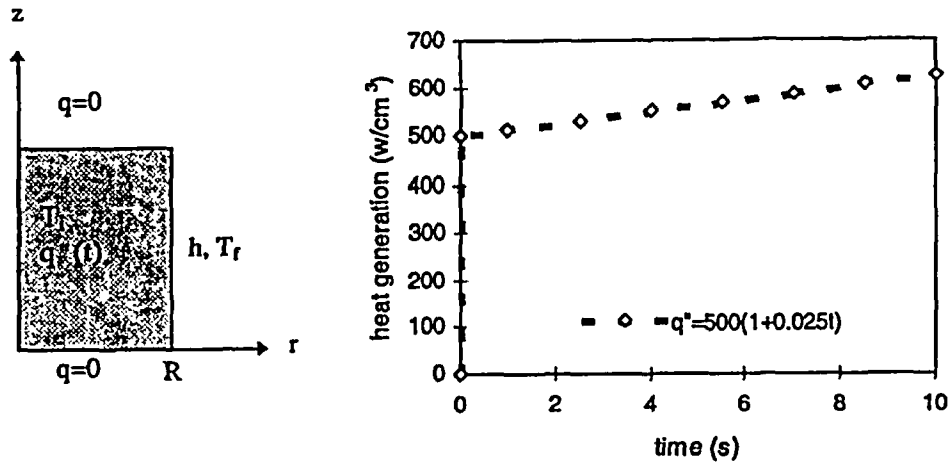

Figure 9 Heat Conduction with Time-dependent Heat Generation (Case 2-9)

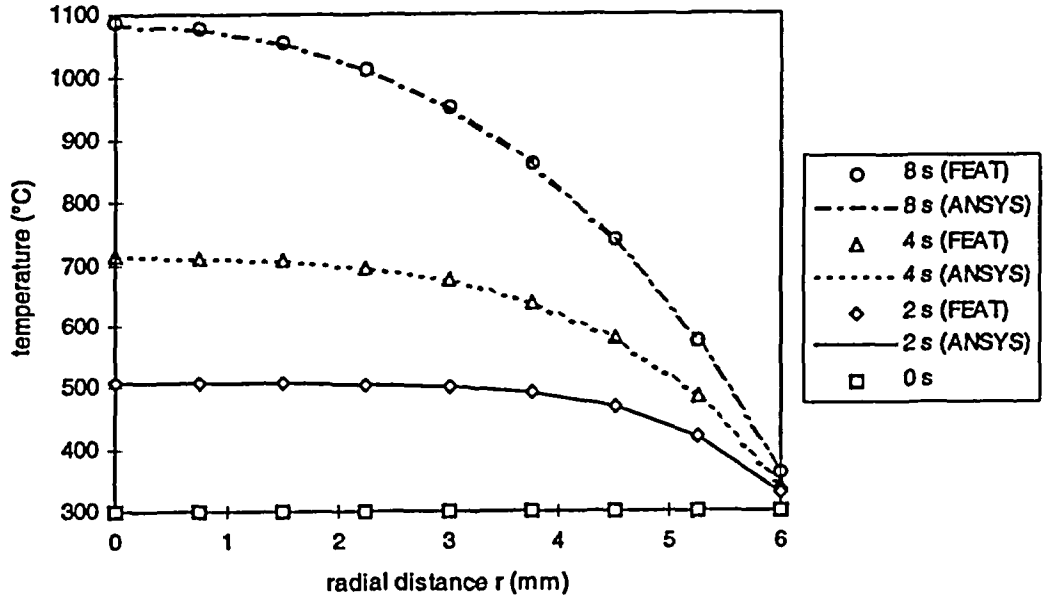

Figure 10 Temperature Profiles for Different Time Instants (Case 2-9)

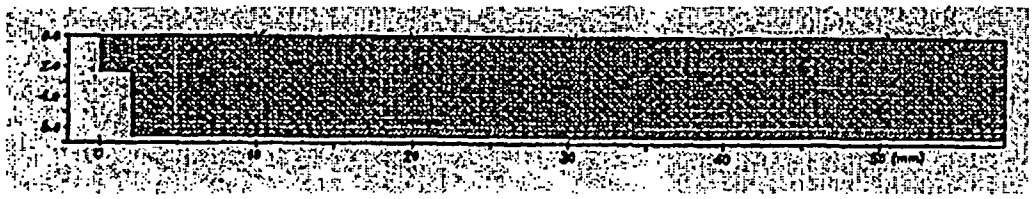

Figure 11 Finite-element Mesh Used for Case 2-14

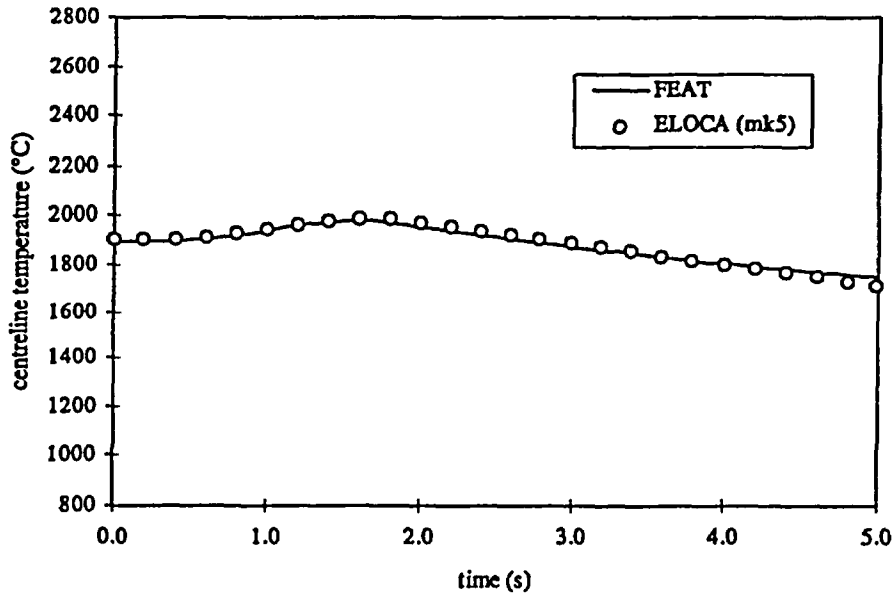

Figure 12 FEAT and ELOCA (mk5)-Predicted Centreline Temperature

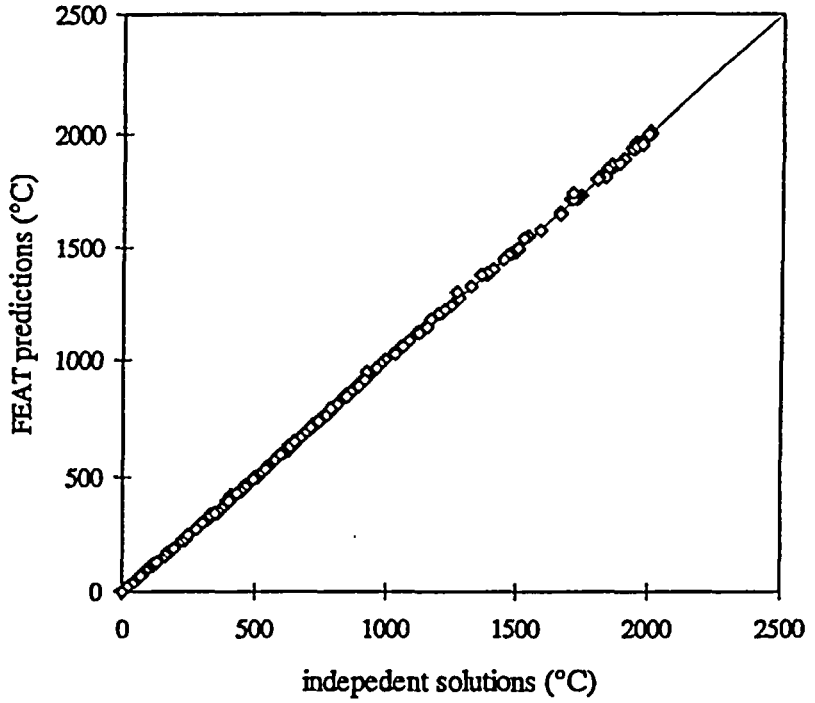

Figure 13 Overall Comparison between FEAT Predictions and Independent Solutions

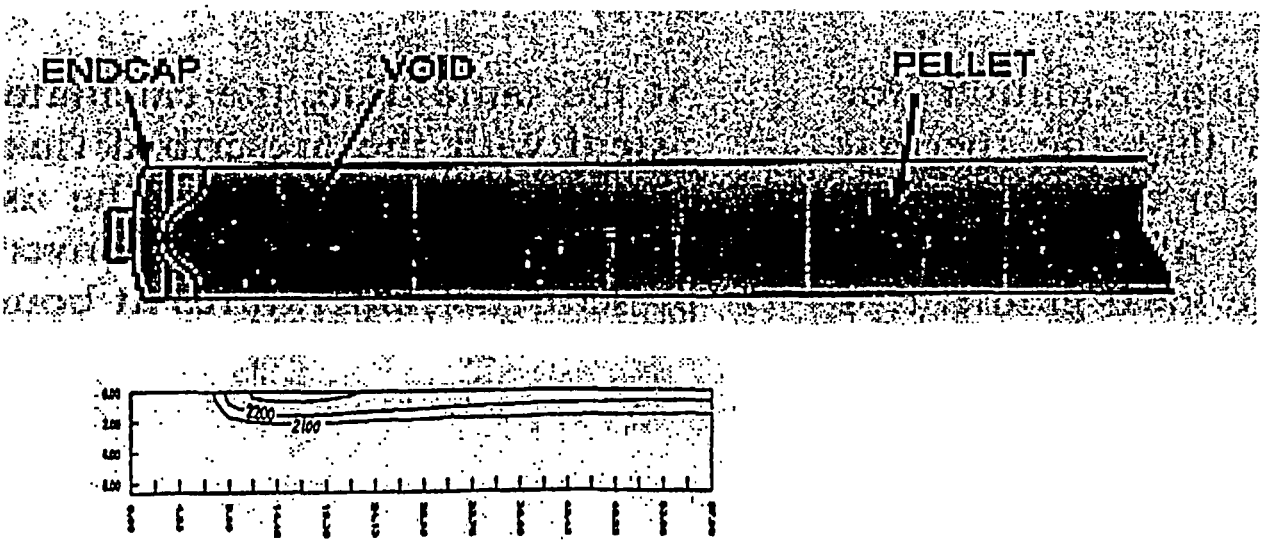

Figure 14 End-Flux-Peaking–Induced Tear-Drop—Shaped Void (top: observed, bottom: predicted) case 3-2

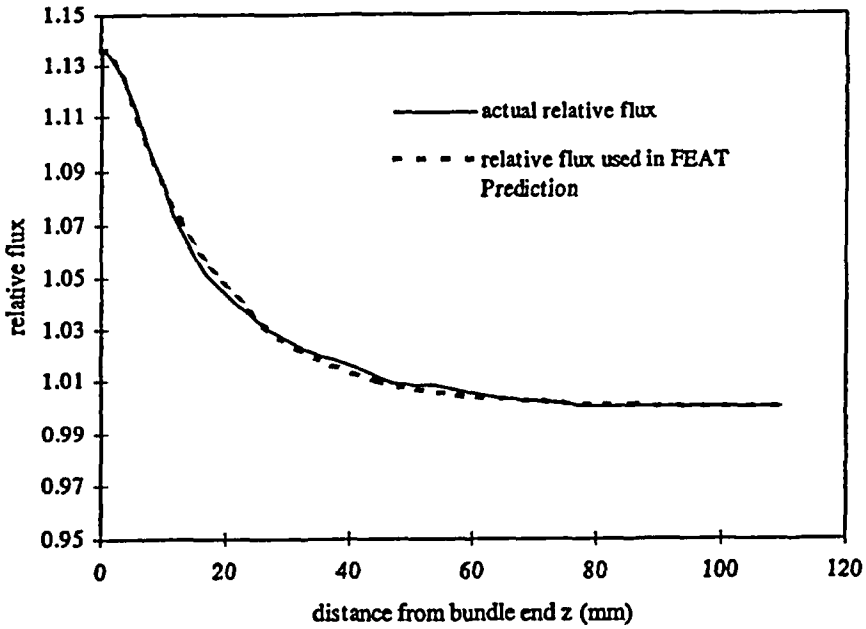

Figure 15 End Flux Peaking Profile

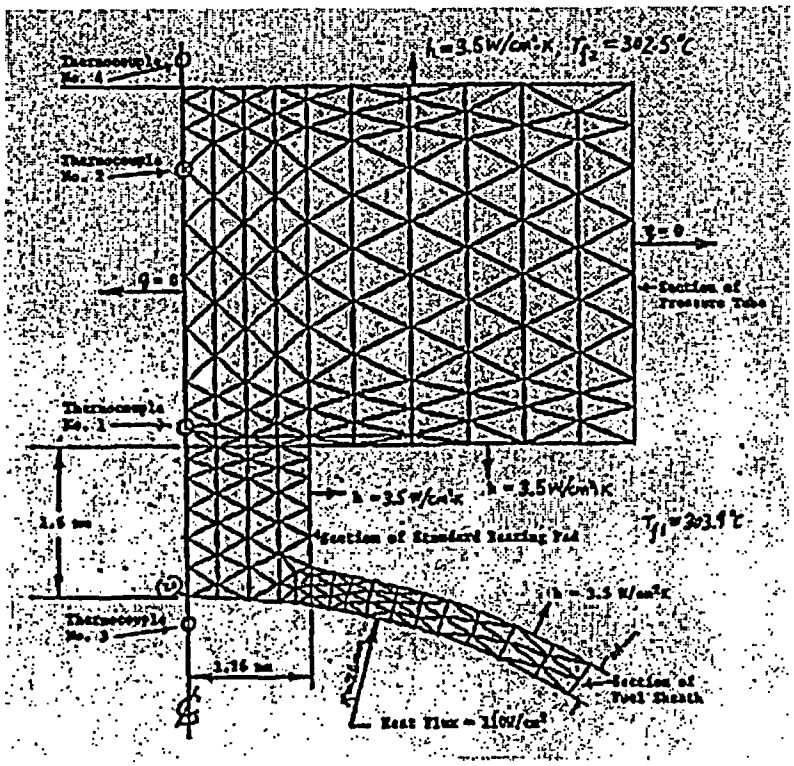

Figure 16 Thermocouple Measurement near Sheath—Bearing-Pad Interface (case 3-3)

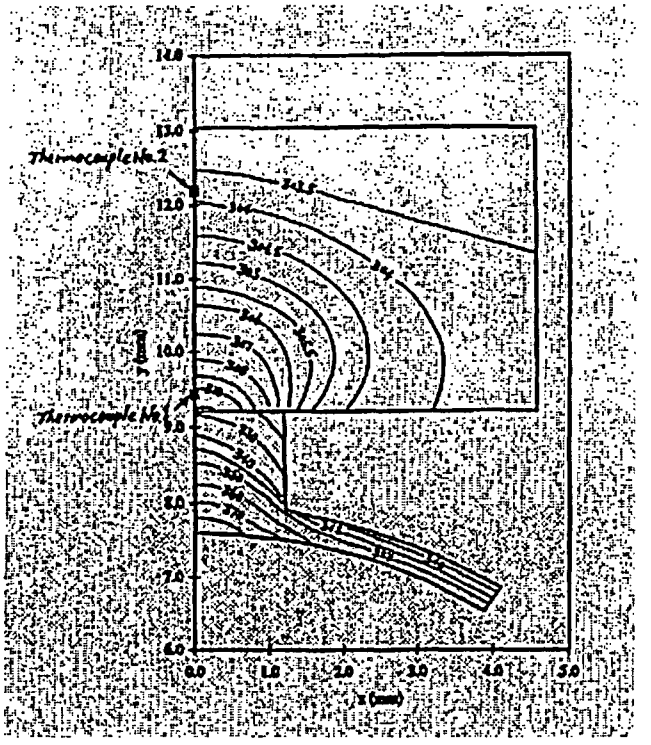

Figure 17 Predicted Isotherms near Sheath Bearing-Pad Interface

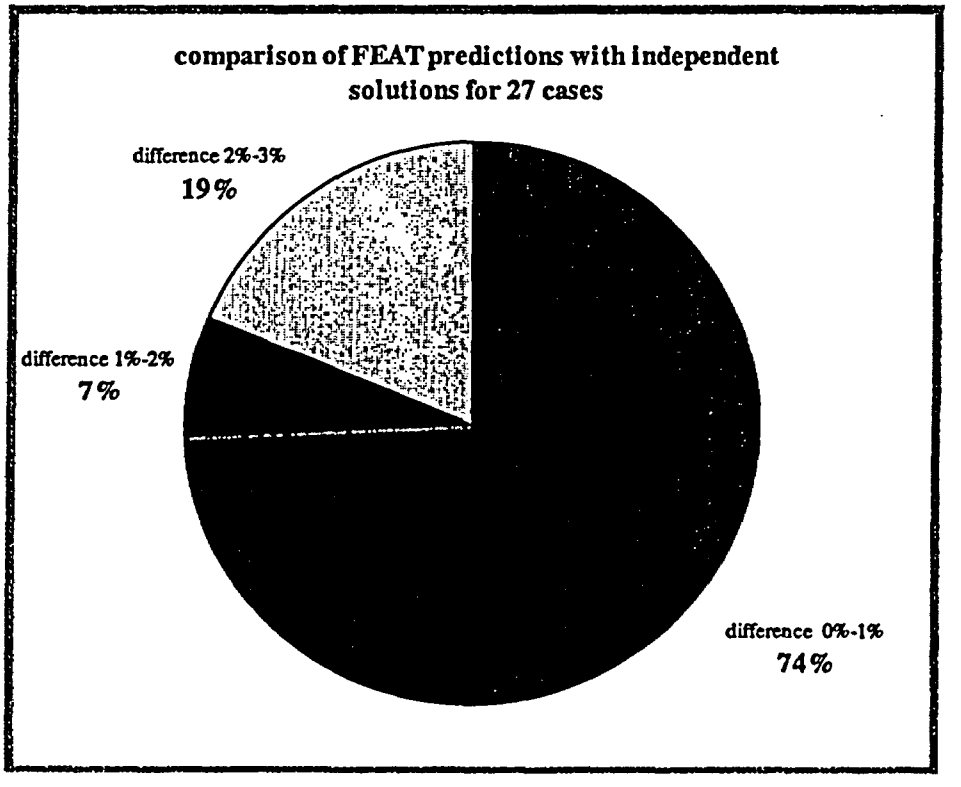

Figure 18 Comparison of FEAT Predictions with Independent Solutions for 27 Cases